Delft University of Technology

Towards Tm^{2+} in sialon thin films grown by sputtering using the gradient deposition

Bosco, Giacomo; Van Der Kolk, Erik

DOI
10.1149/09702.0017ecst

Publication date
2020

Published in
237th ECS Meeting

Citation (APA)
Bosco, G., & Van Der Kolk, E. (2020). Towards Tm^{2+} in sialon thin films grown by sputtering using the gradient deposition. In P. Mascher, F. Rosei, & D. J. Lockwood (Eds.), *237th ECS Meeting: Nanoscale Luminescent Materials 6* (2 ed., Vol. 97, pp. 17-26). IOP Publishing. https://doi.org/10.1149/09702.0017ecst

Important note
To cite this publication, please use the final published version (if applicable).
Please check the document version above.

Copyright
Other than for strictly personal use, it is not permitted to download, forward or distribute the text or part of it, without the consent of the author(s) and/or copyright holder(s), unless the work is under an open content license such as Creative Commons.

Takedown policy
Please contact us and provide details if you believe this document breaches copyrights.
We will remove access to the work immediately and investigate your claim.

This work is downloaded from Delft University of Technology.
For technical reasons the number of authors shown on this cover page is limited to a maximum of 10.

Towards Tm^{2+} in Sialon Thin Films Grown by Sputtering Using the Gradient Deposition

Giacomo B. F. Bosco[a] and Erik van der Kolk[a]

[a] Luminescence Materials Research group, Department of Radiation Science and Technology, Faculty of Applied Sciences, Delft University of Technology, 2629 JB Delft, The Netherlands

The valence stability parameter (E_{Ff}), defined as the difference between the charge transfer energy to the host intrinsic Fermi energy, was used as criterion to analyze the capability of different host materials within the SiAlON class to stabilize divalent thulium. Available data on charge transfer energies and optical bandgap values are reviewed for Si_3N_4, SiO_2, AlN, and Al_2O_3. In addition, new data on thin films, collected by our gradient sputter deposition and characterization method on silicon and aluminum nitrides ($Si_{0.75x}Al_{1-x}N$), are reported. These data are sufficient to show that, at least in the nitride subsection of the SiAlON class, divalent thulium is not expected to be stable due to the presence of high E_{Ff} values. The use of sub-stoichiometric silicon nitride and oxide is also briefly considered.

Introduction

Among different candidates of next generation luminescence solar concentrators (LSC) materials for electricity generating glass applications, divalent thulium (Tm^{2+}) doping has been shown to have a high potential. It has been reported to have 65% absorption of the solar spectral range when in di-halide hosts while showing no self-absorption and a relatively neutral color (1). These characteristics are possible because Tm^{2+} has a strong absorption from the UV up to 900 nm generated by intense $4f^{13} \rightarrow 4f^{12}5d^1$ electronic transitions and a single emission line in near infrared (NIR) at 1140 nm credited to the $^2F_{5/2} \rightarrow {}^2F_{7/2}$ transition of the $4f^{13}$ configuration. However, this specific oxidation state of thulium is rather anomalous: except from SrB_4O_7 (2), it was only stabilized so far on di-halide crystals. These crystals are very hygroscopic in nature and therefore not sufficiently attractive for scaling up in industry standard thin film growth techniques. Thus, it is paramount to extend the list of host materials beyond the halides that can host such a promising optically active element with material classes standard to industry. Host materials pertaining to the SiAlON family have the advantage of being wear resistant, and highly stable to temperatures and thermal shock. The possibility of merging a wide absorption range in the UV-VIS with a narrow emission line in NIR with a host material standard to industry shows high scalability potential.

Rare Earth Valence Stability

When accessing the potential of a given material to host the divalent oxidation state of a given rare earth (RE) ion, one of the accepted and general criteria is given by the E_{Ff} parameter suggested by Dorenbos in 2005 (3) defined by:

$$E_{Ff} = E^{CT} - E_{F,i} \quad [1]$$

In which E^{CT} stands for the charge transfer energy of the trivalent ion (4), interpreted as the energy difference ascribed to the effective removal of one electron from the valence band to the ground state of the divalent ion. $E_{F,i}$ is intrinsic Fermi energy. This relation, essentially borrowed from impurity ionization statistics used in semiconductors, was empirically observed to be a good indicator for RE reduction in solids as well. Without tackling the problem from a first-principles perspective, Dorenbos correlated valence stability of the lanthanides – i.e., the possibility of observing the divalent form of a given lanthanide ion – over more than 300 crystalline compounds to the distance of the lanthanide ground state within the host bandgap and its $E_{F,i}$ (estimated to be at the middle of the valence and conduction bands). In his work, the intrinsic Fermi energy is determined from the host exciton energy through $E_{F,i} = 0.54E^{ex}$.

The main observation in this set of compounds is that a necessary condition for which Eu^{2+} can be found is $E_{Ff} < 0.7$ eV. In this situation, it is reported that Eu^{2+} can be obtained even under oxidizing conditions. $E_{Ff} < 0.7$ eV will be referred to from now on as "Dorenbos' criterion". However, there is no apparent sharp line dividing the situations where a lanthanide ion can be found in a divalent or in a trivalent state. Moreover, if $E_{Ff} > 1.2$ eV, it was reported that "a complete reduction to Eu^{2+} is not possible anymore". This does not necessarily mean that Eu^{2+} cannot be found but that it requires extreme reducing treatments – which can also mean that such a condition might not be stable. Similar arguments can be raised for the case of the next ions most easily reduced (in order they are Yb, Sm, and Tm). Furthermore, this analysis does not allow for a complete quantification of the mixture of oxidation states or the expected average oxidation state.

One of the most relevant tools developed for the interpretation of lanthanide luminescence spectroscopy over the last one and a half decade was the emergence of band diagrams which included the lanthanide 4*f* energy levels (5,6). Those diagrams use optical spectroscopy data such as photoluminescence emission and excitation and sometimes absorption spectroscopy to determine charge transfer energies (4) and optical bandgap information which can then be ascribed, in a simplified picture of the electronic structure of solids, to the RE 4*f* and *5d* (7) levels in both divalent and trivalent oxidation states. This information can also be correlated either relatively to the host valence band edge or to the vacuum energy. Diagrams obtained in such a way are often referred to as host referred binding energy (HRBE) diagrams or vacuum referred binding energy (VRBE) diagrams.

Thus, a first attempt of obtaining criteria for searching possible material candidates hosting Tm^{2+} one could use Dorenbos' criterion on available data regarding the simplest material options within the SiAlON class like SiO_2, Si_3N_4, AlN and Al_2O_3. One of the advantages of the VRBE schemes, or more specifically, the zig-zag shape of the

lanthanide energy levels, is that optical spectroscopy information about one ion of the RE family can offer information about what are the expected charge transfer, 5*d*, and excitation energies of a different RE ion in the same material. Therefore, information on Eu^{2+} and Sm^{3+} charge transfer and $4f \rightarrow 5d$ transition energies are already enough for evaluating if the same compound can stably host Tm^{2+}.

Without the aim of being an exhaustive review on the topic of RE reduction in solid compounds, this paper contributes by discussing relevant literature and the progress made so far towards unravelling conditions for obtaining the rather anomalous Tm^{2+} in hosts pertaining to the SiAlON class. This is undertaken through the deliberate choice of Dorenbos' criterion to search and analyze for promising compositions and, thus, optical properties.

In the next section, a survey of a selection of available data of the materials from the corners of the SiAlON phase diagram, i.e., SiO_2, Si_3N_4, Al_2O_3, and AlN, are reviewed for the presence of Eu^{2+} and Sm^{2+} and correlated with Dorenbos' criterion. This data is then correlated with the ability to host Tm^{2+} and with the expected effect of sub stoichiometry on the promotion of divalent formation.

This discussion is followed by experimental results on the feasibility for obtaining Tm^{2+} in the nitride composition region of the SiAlON class. Tm^{3+} excitation and emission photoluminescence were correlated with Dorenbos' criterion for a wide ratio of Al/Si. The films were prepared by combinatorial RF/DC magnetron sputtering and characterized as a function of position on the substrate through the gradient method (8).

Finally, a small section is dedicated to exploring the implications of recent results available on the VRBE diagrams of sub-stoichiometric SiO_2 and Si_3N_4 in the promotion of Tm^{2+}.

Optical Spectroscopy data on Eu and Sm

In TABLE I there is a collection of available data on charge transfer (E^{CT}), exciton energy (E^{ex}), and the estimated E_{Ff} parameters for Eu, Sm, and Tm doped in Si_3N_4, AlN, SiO_2 and Al_2O_3. E_{Ff} is more easily accessible for Eu than for the other two dopants. For Sm and Tm, E_{Ff} can be easily estimated by shifting these energies by 1.2 eV for Sm^{2+}, and 1.7 eV for Tm (9). The results contained in TABLE I are schematically gathered in Figure 1.

There is no direct lanthanide spectroscopic data on the CT energies for SiO_2. But a reasonable estimate can be done looking at the trends found in different oxide compounds. The E^{CT} depends, in a first approximation, on the binding strength and distance experienced by the lanthanide to the anions it is bonded to (10). Additionally, it increases with E^{ex}. In the $LiRESiO_3$ series of elements, oxygen is bonded in SiO_4^{4-} tetrahedra which can resemble the neighborhood expected for Eu^{3+} in SiO_2. The compound with highest E^{ex} is $LiLuSiO_4$, thus, a reasonable estimate on Eu^{3+} CT energy would lie on similar levels found for $LiLuSiO_4$:Eu, i.e., ~5.5 eV. There is direct data on the Eu^{3+} CT in Al_2O_3. It has been reported to be 3.8 eV (11). Characterization of bandgap energies from XPS results on different Al_2O_3 phases gives 8.1 eV for α-Al_2O_3, 7.0 eV for γ-Al_2O_3, and 6.5 eV in amorphous Al_2O_3 (12,13). Using the assumption that the charge transfer energy

does not strongly change in alumina polymorphs (14) one can estimate the different E_{Ff} values for Al_2O_3. The lowest E_{Ff} value for Eu, which can be correlated to the higher chances of reducing a RE ion, occurs for α-Al_2O_3. In fact, Eu^{2+} can be observed in α-Al_2O_3 (15) but it is not commonly observed in amorphous SiO_2 (16,17). Even in the case of higher E_{Ff} values, Eu^{2+} can still be observed in SiAlONs (28-20) and in γ-Al_2O_3 (11). In all cases, Dorenbos' criterion is satisfied. Despite the high E_{Ff} value retrieved for Sm in γ-Al_2O_3, Sm^{2+} can still be observed in γ-Al_2O_3 (21).

In the nitrides, the charge transfer energies of Eu^{3+} are relatively close to each other (10). For the same reasons discussed above, E^{CT} in Si_3N_4 should be lower than the value known for AlN – ~3.5 eV (22). This can be estimated to be ~ 3.2 eV, similar to what has been found in GaN (23). So, E_{Ff} are respectively at 0.6 and 0.1 eV, meeting Dorenbos' criterion in both cases. However, Eu tends to be trivalent in AlN (22) but can also be found in divalent form (24). In Si_3N_4 (25) Eu is known to have a mixed valence. Eu^{2+} characteristic luminescence is known to be stable in a-Si_3N_4 even after post deposition thermal treatments on oxidizing conditions. As previously mentioned, Dorenbos' valence stability model is an empirical relationship which can particularly fail in situations where E_{Ff} is around 0.7 eV, e.g., when Eu is doped in the Si_3N_4 (25) or AlN (22). Moreover, the inherent error bars associated with positioning the energy levels within the forbidden bandgap (26) should be taken into account and, very probably, can be an additional limiting factor to the inefficiency in the method to correctly predict the presence of Eu^{2+}.

TABLE I. Charge transfer (E^{CT}), exciton energies (E^{ex}), and the estimated E_{Ff} parameter for Eu, Sm, and Tm in the simple materials contained in the SiAlON class.

Host	RE	$E^{CT}(3+)\ [eV]$	$E^{ex}\ [eV]$	$E_{Ff}\ [eV]$
	Eu	3.2[b]	4.8[a]	0.6
Si_3N_4	Sm	--		1.8
	Tm	--		2.3
	Eu	3.5[d]	6.2[d]	0.1
AlN	Sm	--		1.3
	Tm	--		1.8
	Eu	5.5[j]	8.7[i]	0.8
SiO_2	Sm	--		2.0
	Tm	--		2.5
	Eu	3.8[e]	8.1[c]	-0.6
α-Al_2O_3	Sm	5.0[f]		0.6
	Tm	--		1.1
	Eu	3.8[e]	7.0[g]	0.0
γ-Al_2O_3	Sm	5.0[f]		1.2
	Tm	--		1.7
	Eu	3.8[e]		0.3
Amorp. Al_2O_3	Sm	5.0[f]	6.5[h]	1.5
	Tm	--		2.0

[a] Estimated using the optical bandgap value of 5.2 eV (27) by $E^{ex} = \frac{E_g}{1.08}$; [b] Estimated from GaN (28); [c] Estimated using bandgap value of 8.7 eV (12) - more information on the text; [d] From (28); [e] Estimated using excitation spectra results from (11). An assumption about the CT energy not changing drastically for all alumina polymorphs is made. [f] Estimated using excitation spectra results of (21); [g] Estimated using XPS results from $E_g = 7.6\ eV$ (18); [h] Estimated using XPS results from $E_g = 7.0\ eV$ (13); [i] From (29); [j] Estimated from $LiRESiO_4$ series as suggested in (10) – more information is in the text.

As previously mentioned, the higher the bandgap and the lower the charge transfer energy of the trivalent ion, the better the chances of a candidate material to stably host

Tm^{2+}. As suggested from these results, the simplest compounds, within the SiAlON phase diagram, do not show the necessary conditions for hosting Tm^{2+}, i.e., a high optical bandgap and a low charge transfer energy of the trivalent ion. For all materials, the E_{Ff} values expected for Tm are well above 1.0 eV. Among those options, the best one would be α-Al_2O_3 with an E_{Ff} of 1.1 eV which is still 0.4 eV above the Dorenbos' criterium of 0.7 eV.

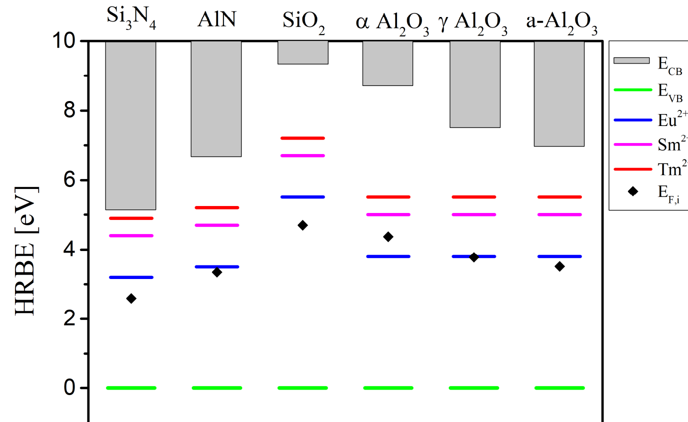

Figure 1. Host referred binding energy (HRBE) diagrams of the simple compounds within the SiAlON class constructed from values in TABLE I. The lines in blue, pink and red represent the ground state energy levels occupied respectively in Eu^{2+}, Sm^{2+} and Tm^{2+}. The green lines represent the valence band edge location and the grey rectangles the location of the conduction bands.

Valence stability of Tm in $SiAlN_x$:Tm^{3+}

In order to directly access the influence of the Al/Si ratio in silicon and aluminum nitrides ($Si_{0.75x}Al_{1-x}N$ for short) on the stabilization of Tm^{2+}, the gradient characterization method (8) was used to relate local (that is position dependent) film composition – determined by energy dispersive x-ray spectroscopy (EDX) – with local transmission, photoluminescence emission and excitation data. This unique approach made it possible to retrieve a wide composition range in just a handful of different films.

Experimental

Amorphous thin films of Tm doped in $Si_{0.75x}Al_{1-x}N$ were prepared by combinatorial magnetron RF/DC sputtering. Four films were deposited on square 50×50 mm² UV grade quartz substrates within an AJA ATC Orion 5 magnetron sputtering system with a base pressure of 1.5×10^{-7} torr. Prior to the deposition, each substrate had been cleaned by rinsing trice with DI water and ethanol. The deposition was carried out with 5.08 cm diameter metal Tm (99.99%, Demaco), Si (99.999%, Lesker), and Al (99.9995%, Lesker) targets which were reactively co-sputtered. The process total gas flow was kept fixed at 32 sccm. 6N purity Ar and 5N purity N_2 gas flows were chosen to meet the requirements in stoichiometry and deposition rate. TABLE II shows the deposition parameters used for the fabrication of each film. The working pressure was 3×10^{-3} torr and the samples were not actively heated.

Transmission, photoluminescence emission and excitation were carried out with the methods described in detail elsewhere (8). Composition characterization were carried out from SEM-EDS collected from a JEOL JSM-IT100 operated at 15 kV with probing current at 50% for 2 min per measurement. Elemental composition was quantified at 1000× magnification. Low vacuum mode (at 35 Pa) was used for to enhance quantitative elemental analysis without the need for a conductive coating. The signal and elemental composition was then compared with simulations carried out with DTSA II software for additional consistency considering the signal from the quartz substrates was also present.

TABLE II. Deposition conditions used for each film.

Film	Power Employed			Gas Flow	
	Si [W]	Al [W]	Tm [W]	Ar [sccm]	N_2 [sccm]
Si_3N_4	130	0	10	27	5
AlN	0	110	25	22	10
Library 1	110	60	20	22	10
Library 2	90	64	30	22	10

Results

Figure 2a shows a top view perspective of the metallic precursors used for film fabrication. Figure 2b shows the appearance of the library 1 film right after deposition. Figure 2c shows a surface map of the expected local composition of library 1. Interpolation was carried out using the surface-source evaporation equation (8) to extend the [Al]/([Al]+[Si]) ratio over all substrate – shown as a “heat” map between 0 (blue) and 1 (yellow). Figure 2d shows a surface map representing the distribution of the local thickness obtained from transmission in VIS region. Figure 2e is the typical photoluminescence emission spectrum of Tm^{3+} which were used to generate the excitation plots shown in Figure 3.

Figure 3a shows the excitation spectrum obtained from the Si_3N_4:Tm thin film. Figure 3b is the excitation spectrum upon one point at library 2. Figure 3c shows the excitation of AlN:Tm. Eu^{3+} CT energy in Si_3N_4 is known to be at 3.2 eV. This results in an approximate position of Tm^{3+} CT energy to be at 4.9 eV. The optical bandgap (E^{04} definition) of Si_3N_4 is around 5.2 eV (30). Thus, photoluminescence excitation curve fitted to a single Gaussian (Figure 3a) can be interpreted as the convolution of the CT and exciton excitation. The CT energy of AlN:Tm have already been characterized before to the band centered at ~4.5 eV (31). The inset shows the transition assigned to AlN exciton at 6.2 eV. Similar excitation spectra were collected in various locations of libraries 1 and 2 to directly access the influence of [Al]/([Al]+[Si]) on the Tm^{3+} CT energy. The graph shown in Figure 3d evidences that the CT band energy in the nitrides hardly changes with the Al/Si ratio remaining close to $4.8\ eV$.

Using values from TABLE I it is possible to estimate E_{Ff} to have a very high value for AlN ($E_{Ff} \equiv E^{CT} - 0.54E^{ex} \approx 1.3\ eV$) and for Si_3N_4 ($E_{Ff} = 2.1\ eV$). In the $Si_{0.75x}Al_{1-x}N$ alloy, E_{Ff} is expected to be even higher due to a bandgap contraction with higher Si content and a very similar E^{CT}. This indicates that obtaining Tm^{2+} in this region of the SiAlON phase space might indeed not be possible.

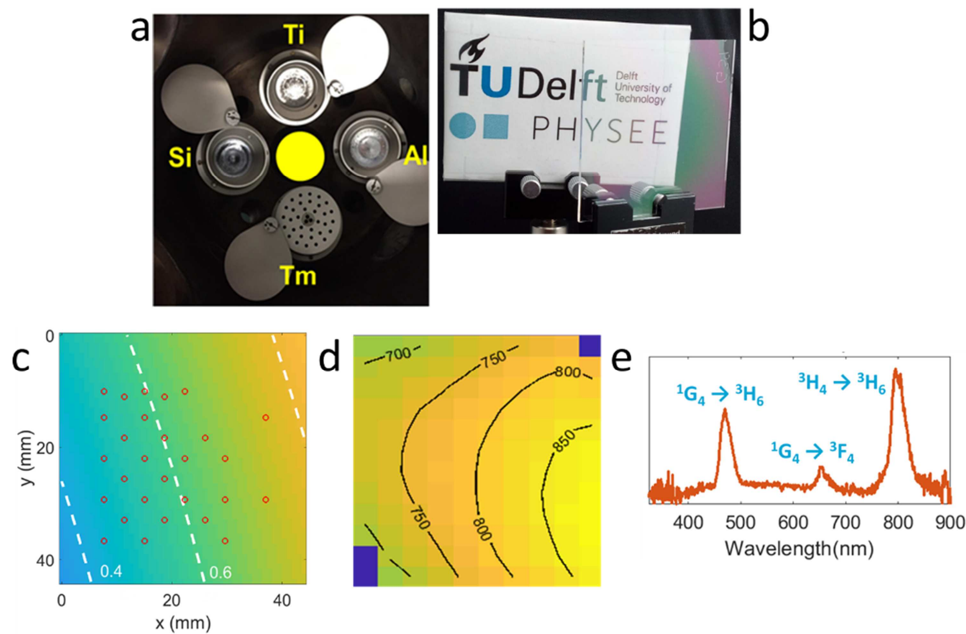

Figure 2. a) Top view of the 4 sputtering guns employed in the combinatorial sputtering system. The yellow circle indicates the position of the substrate relative to the guns. Ti gun was used only for assuring vacuum quality. A metallic "mask" is used over Tm gun to limit its deposition rate; b) Picture of library 1; c) Distribution of the relative concentration of Al over Al and Si - [Al]/([Al]+[Si]) - as obtained by EDS analysis (red points indicate measured positions; color map is the result of evaporation curve fitting method (8,32)); d) Thickness (in nm) distribution of library 1 as obtained by transmission analysis; e) Typical Tm^{3+} emission spectrum obtained in $SiAl_{1-x}N_x$ thin gradient films showing the transitions $^1G_4 \rightarrow {}^3H_6$, $^3F_4$, and $^3H_4 \rightarrow {}^3H_6$.

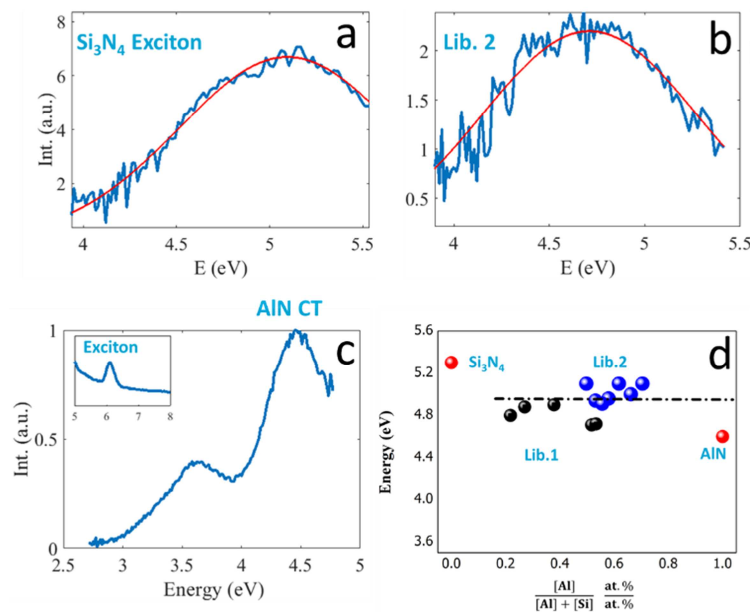

Figure 3. a) Room temperature excitation spectra (blue) and Gaussian fit (red) of the Tm^{3+} $^3H_4 \rightarrow {}^3H_6$ line in Tm^{3+} doped Si_3N_4; b) PLE spectra in one point in library 2; c) and in AlN thin films; d) PLE peak energy (correlated with Tm CT energy) vs. [Al]/([Al]+[Si]) obtained from a selected regions in a series of gradient films.

Sub-stoichiometry as strategy of Tm reduction

Rather than tuning only the cation by replacing Si for Al, a different strategy would be to study the influence of the O or N anion ratio. Since the charge transfer energy of RE^{3+} depends on the energy difference between the valence band edge and the RE^{2+} energy level, a change in the oxygen (or nitrogen) deficiency in the host material can alter the position of the valence band edge while maintaining the RE energy levels relatively unchanged (4). This lowers the required charge transfer energy offering better chances of a given material for hosting Tm^{2+} because this effectively raises the Fermi energy moving it closer to the 2+ ground state in the VRBE diagram.

In this section, this possibility is shortly discussed because tight-binding calculations results on the electronic structure, as a function of oxygen (or nitrogen) content in sub stoichiometric Si_3N_4 (27) and SiO_2 (32), have become recently available.

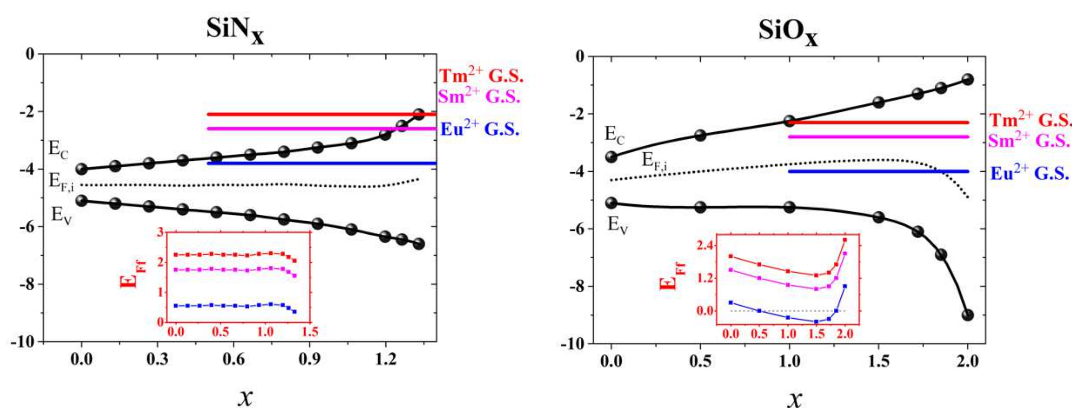

Figure 4. Effect of the nitrogen – or oxygen– ratio over Si on the optical bandgap calculated by a tight binding method in SiO_x (32) and SiN_x (27). The dashed lines indicate the expected intrinsic Fermi energy located at the midpoint of the bandgap. The insets show explicitly the dependence of the E_{Ff} parameter upon x. The colored lines indicate the ground state levels of Eu^{2+} (in blue), Sm^{2+} (in pink), and Tm^{2+} (in red). These positions are placed on the bases of what is known for Si_3N_4 and SiO_2 and are assumed to not change over stoichiometry.

Figure 4 is an adapted plot of the trends in the VRBE of E_V and E_C band edges as a function of the stoichiometry of those compounds. The same references used in TABLE I for Si_3N_4 and SiO_2 are used to place the VRBEs of the ground state levels related to Eu^{2+}, Sm^{2+}, and Tm^{2+}. Because the chemical shift (which determines the VRBE of the RE energy levels) depends, in a first approximation, only on the first shell of anions bonded to the RE (14), the dependence of these levels with the stoichiometry is not strong, so it seems a good approximation to fix these energies across the stoichiometry. The inset of each graphic shows the estimated E_{Ff} values as a function of stoichiometry. For the sub-nitrides (SiN_x), E_{Ff} is always positive for all the ions showing a minimum value in the stoichiometric Si_3N_4, so the sub-stoichiometry strategy does not have a positive result in RE reduction. For the sub-oxides (SiO_x), however, there is a minimum in the E_{Ff} value close to $x = 1.5$. In this situation, E_{Ff} is expected to be negative for Eu, ~0.8 eV for Sm, and ~1.3 eV for Tm. It is known that Sm^{2+} is not stable in SiO_2 but photoluminescence attributed to it can be observed in $SiO_{1.2}$ after annealing on oxidizing atmosphere (33). This is also consistent with recent observations with the raise in Sm^{2+} concentration, determined by XPS, in near-stoichiometric Sm doped SiO_2:Al materials (34). The lowest

E_{Ff} value experienced by Tm^{2+} seems already too high for any measurable amount of Tm^{2+}. Thus, this strategy alone might not be enough for the formation of Tm^{2+}.

Conclusion

The work presented in this paper shows the current status of an ongoing effort on the determination of a suitable host material capable of stably hosting Tm^{2+} while still being compatible with current installed industry infrastructure – in particular, this paper presented a Tm^{2+} valence stability study focused on materials within the SiAlON class. An attempt of reviewing relevant data for defining new strategies of preparation of these materials was delivered and an analysis was given in terms on what have been referred here as the Dorenbos' criterion.

According to the available data on Si_3N_4, SiO_2, AlN, and Al_2O_3, mixed valence Eu and Sm are expected and observed while the conditions for Tm^{2+} formation is not met. Composition and optical characterizations reported on gradient Tm^{3+} doped $Si_{0.75x}Al_{1-x}N$ thin films also suggest that the substitution of Si by Al does not offer the necessary conditions for Tm^{2+} stabilization. Other strategies, such as the fabrication of sub-stoichiometric materials seem to improve the probability of stabilizing Tm^{2+} but at the expense of lowering severely the material bandgap.

Research on the oxides is still under way and might hold a suitable candidate. As suggested by the results collected for SiO_2 and Al_2O_3, the replacement of Si by Al can have a more pronounced effect on the CT energy of Tm^{3+} favoring Tm^{2+} stabilization.

Acknowledgments

G. B. F. Bosco thanks P. Dorenbos and E. P. J. Merkx for the helpful discussions.

References

1. O. M. ten Kate, K. W. Krämer, and E. van der Kolk, *Sol. Energy Mater. Sol. Cells* **140**, 115 (2015).
2. P. Solarz, J. Komar, M. Glowacki, M. Berkowski, and W. Ryba-Romanowski, *RSC Adv.* **7**, 21085 (2017).
3. P. Dorenbos, *Chem. Mater.* **17**, 6452 (2005).
4. P. Dorenbos, *Opt. Mater. (Amst.)* **69**, 8 (2017).
5. P. Dorenbos, *Phys. Rev. B* **87**, 035118 (2013).
6. P. Dorenbos, *ECS J. Solid State Sci. Technol.* **2**, R3001 (2013).
7. P. Dorenbos, *J. Lumin.* **91**, 155 (2000).
8. E. P. J. Merkx and E. van der Kolk, *ACS Comb. Sci.* **20**, 595 (2018).
9. P. Dorenbos, *J. Phys. Condens. Matter* **15**, 8417 (2003).
10. P. Dorenbos, J. Lumin. **111**, 89 (2005).
11. M. A. F. Monteiro, H. F. Brito, M. C. F. C. M. Felinto, G. E. S. Brito, E. E. S. Teotonio, F.M. Vichi, and R. Stefani, *Microporous Mesoporous Mater.* **108**, 237 (2008).
12. R. H. French, *J. Am. Ceram. Soc.* **73**, 477 (1990).
13. E. O. Filatova and A. S. Konashuk, *J. Phys. Chem.* C **119**, 20755 (2015).
14. P. Dorenbos, *Phys. Rev.* B **85**, 165107 (2012).
15. N. Rakov and G.S. Maciel, *J. Lumin.* **127**, 703 (2007).

16. D. Zhang, X. Hu, G. Jing, E. Liu, J. Fan, G. Zhang, and X. Hou, *J. Nanosci. Nanotechnol.* **14**, 3642 (2014).
17. X. Hu, J. Fan, T. Li, D. Zhang, W. Chen, J. Bai, and X. Hou, *Opt. Mater. (Amst).* **29**, 1327 (2007).
18. H. T. Hintzen, J. W. H. Van Krevel, D. De Graaf, R. Metselaar, Y. Menke, and S. Hampshire, *J. Mater. Sci.* **39**, 2237 (2004).
19. R.-J. Xie, N. Hirosaki, M. Mitomo, Y. Yamamoto, T. Suehiro, and K. Sakuma, *J. Phys. Chem. B* **108**, 12027 (2004).
20. E. P. J. Merkx, S. van Overbeek, and E. van der Kolk, *J. Lumin.* **208**, 51 (2019).
21. S. Stojadinović, N. Tadić, and R. Vasilić, *J. Lumin.* **192**, 110 (2017).
22. E. P. J. Merkx, T.G. Lensvelt, and E. van der Kolk, *Sol. Energy Mater. Sol. Cells* **200**, 110032 (2019).
23. P. Dorenbos and E. van der Kolk, *Opt. Mater. (Amst).* **30**, 1052 (2008).
24. K. Inoue, N. Hirosaki, R.J. Xie, and T. Takeda, *J. Phys. Chem. C* **113**, 9392 (2009).
25. L. R. Tessler and G. F. Bosco, *ECS Trans.* **72**, 27 (2016).
26. J. J. Joos, D. Poelman, and P. F. Smet, *Phys. Chem. Chem. Phys.* **17**, 19058 (2015).
27. A. N. Sorokin, A. A. Karpushin, and V. A. Gritsenko, *JETP Lett.* **98**, 709 (2014).
28. P. Dorenbos, *Phys. Rev.* B **87**, 035118 (2013).
29. A. E. R. Malins, N. R. J. Poolton, F. M. Quinn, O. Johnsen, and P. M. Denby, *J. Phys. D. Appl. Phys.* **37**, 1439 (2004).
30. J. Robertson, *Philos. Mag. B* **63**, 47 (1991).
31. H. J. Lozykowski, W. M. Jadwisienczak, A. Bensaoula, and O. Monteiro, *Microelectronics J.* **36**, 453 (2005).
32. A. A. Karpushin and V. A. Gritsenko, *JETP Lett.* **108**, 127 (2018).
33. A. R. Zanatta, *Opt. Mater. Express* **6**, 2108 (2016).
34. C. D. Boers, *SiAlO:Sm Thin-Films An Investigation into the Mechanisms Underlying the Poor Absorption of* Sm^{2+} *and the Poor Thermal Stability of Its Lumi-Nescence*, Delft University of Technology, 2020.